Published in final edited form as:
J Healthc Eng. 2013 ; 4(1): 109–126. doi:10.1260/2040-2295.4.1.109.

Accumulation of Phase-Shift Nanoemulsions to Enhance MR-Guided Ultrasound-Mediated Tumor Ablation In Vivo

Jonathan A. Kopechek, Ph.D.[1], **Eunjoo Park, Ph.D.**[2], **Chang-Sheng Mei, Ph.D.**[2], **Nathan J. McDannold, Ph.D.**[2], and **Tyrone M. Porter, Ph.D.**[1,3,*]

[1]Department of Mechanical Engineering, Boston University, Boston, MA, USA

[2]Department of Radiology, Brigham and Women's Hospital, Harvard Medical School, Boston, MA, USA

[3]Department of Biomedical Engineering, Boston University, Boston, MA, USA

Abstract

Magnetic resonance-guided high intensity focused ultrasound (MRgHIFU) is being explored as a non-invasive technology to treat solid tumors. However, the clinical use of HIFU for tumor ablation applications is currently limited by the long treatment times required. Phase-shift nanoemulsions (PSNE), consisting of liquid perfluorocarbon droplets that can be vaporized into microbubbles, are being developed to accelerate HIFU-mediated heating. The purpose of this study was to examine accumulation of PSNE in intramuscular rabbit tumors *in vivo*. MR images were acquired before and after intravenous injection of gadolinium-containing PSNE. MR signal enhancement was observed in rabbit tumors up to six hours after injection, indicating that PSNE accumulated in the tumors. In addition, PSNE vaporization was detected in the tumor with B-mode ultrasound imaging, and MR thermometry measurements indicated that PSNE accelerated the rate of HIFU-mediated heating. These results suggest that PSNE could dramatically improve the efficiency and clinical feasibility of MRgHIFU.

Keywords

phase-shift nanoemulsion; nanoparticle accumulation; rabbit VX2 tumor; MR-guided HIFU ablation

1. INTRODUCTION

Cancer is the second leading cause of death in the United States. More than 1 in 3 Americans develop cancer during their lifetime [1, 2]. Current standard-of-care includes surgery, chemotherapy, or radiotherapy. Surgery is generally preferred for localized tumors due to the serious systemic side effects often induced by chemotherapy and radiotherapy. However, surgery is limited to resectable tumors and many advanced tumors are inoperable. Several minimally invasive treatments have been developed for non-resectable solid tumors, which kill cancer cells by rapidly heating or freezing the tumor using microwaves, radiofrequency waves, lasers, or cryogens such as liquid nitrogen [3]. However, these

[*]Corresponding author: Tyrone M. Porter, Ph.D., Departments of Mechanical Engineering and Biomedical Engineering, Boston University, 110 Cummington Mall, Boston, MA 02215. Phone: (617) 353-7366. tmp@bu.edu. .
Other authors: jonathan.kopechek@gmail.com; eunjoo.park@gmail.com; meic@bwh.havard.edu; njm@bwh.harvard.edu.

CONFLICT OF INTEREST
The authors have no conflicts of interest.

techniques generally require interstitial energy sources, which can cause complications from visceral and vascular puncture or tumor reseeding [4, 5]. To overcome these challenges, magnetic resonance-guided high intensity focused ultrasound (MRgHIFU) has been explored as a non-invasive technology to treat solid tumors.

High intensity focused ultrasound (HIFU) can be used to heat tissues rapidly and locally, forming lesions of coagulated tissue with millimeter precision [6-12]. Ultrasound waves can pass through the skin and soft tissue without causing damage outside of the focal volume. HIFU is currently FDA-approved for treatment of uterine fibroids and is also being investigated clinically to thermally ablate tumors of the breast [13, 14], pancreas [15], liver [16, 17], kidney [16, 18], and prostate [19-21]. Non-invasive imaging is used to detect the location and boundary of the tumor and guide the placement of the ultrasound focus within the tumor. Magnetic resonance imaging (MRI) has been used extensively to guide HIFU treatments due to its high spatial resolution and contrast [22]. In addition, MRI-based thermometry can be used to measure temperature variations during the HIFU treatment [23-30]. Thus, MRI is useful for treatment planning and monitoring of HIFU treatment.

The clinical use of HIFU for tumor ablation applications is currently limited by the long treatment times (on the order of hours) and high acoustic powers required. Lesions formed by HIFU ablation are typically less than 10 mm^3; thus, multiple lesions must be formed sequentially to ablate the entire tumor volume. In order for HIFU ablation therapy to become clinically feasible, the treatment times must decrease by increasing the heating rate and/or lesion volumes achieved with each ultrasound exposure. In addition, adverse events including skin burns have been reported as a result of the high power required for consistent lesion formation [31, 32]. Thus, reducing the acoustic power needed for lesion formation would also improve the clinical utility of HIFU ablation therapy.

It has been shown that microbubbles can be used to accelerate ultrasound-mediated heating and lesion formation [33-39]. At sufficiently high acoustic pressures, ultrasound can cause bubbles to oscillate non-linearly followed by a violent collapse known as inertial cavitation, resulting in acoustic emissions across a broad range of frequencies. Tissue absorption of acoustic energy is converted into heat, which increases with acoustic frequency. Thus, the high-frequency acoustic emissions from inertial cavitation accelerate heating within tissue. Studies in tissue-mimicking gel phantoms [34], and in *ex vivo* [33], and *in vivo* tissue [35] have demonstrated a dramatic increase in the measured heating rate and peak temperature in the presence of acoustic cavitation. These results indicate that microbubbles can be used to reduce the time required for thermal ablation.

Because bubbles are not readily available in tumors, they must be formed or introduced into the tissue. A common approach for introducing microbubbles is to systemically administer ultrasound contrast agents (UCA), which are microbubbles coated with a lipid, protein, or polymer shell, before ultrasound exposure [37, 38, 40-42]. However, microbubbles injected into the bloodstream remain in circulation and do not accumulate within the tumor due to their size [43-45]. The circulating bubbles can increase the absorption of ultrasound in tissue along the path of the propagating waves, potentially causing unwanted heating and irreversible thermal damage to healthy tissue surrounding the targeted tumor. Alternatively, bubbles can be formed locally within the tumor using very high amplitude acoustic pulses [46-49]. However, the production of bubbles in tumors using ultrasound pulses can vary significantly due to the heterogeneity of tumor tissue, making it difficult to reliably control bubble formation. Furthermore, it has been documented that the pressure threshold for bubble formation in tissue without nuclei can exceed 10 MPa [48, 49], and controlling bubble formation temporally and subsequent oscillations at these pressures is extremely difficult. Phase-shift nanoemulsions (PSNE) present a potential solution to these challenges.

PSNE are suspensions of lipid- or albumin-coated liquid perfluorocarbon droplets (Figure 1) which exist in a superheated state, such that the surface tension of the droplet shell prevents vaporization of the liquid perfluorocarbon core even at temperatures above the bulk perfluorocarbon boiling point. Ultrasound pulses can be used to induce a phase change in the emulsion droplets in response to the rarefactional part of the pressure wave, converting the liquid droplets into gas-filled microbubbles [50-52].

In general, blood vessels in tumors are inherently leakier than normal vessels. Thus, nanoparticles can preferentially accumulate in tumors by passing through fenestrations in the tumor vasculature, a phenomenon known as the enhanced permeability and retention (EPR) effect [53, 54]. In contrast to exogenous microbubbles that are generally a few microns in diameter, liquid droplets can be produced with diameters of 200 nm or less in order to achieve passive accumulation in tumors through the EPR effect [55, 56]. After accumulation of PSNE in the tumor, short ultrasound pulses of sufficient pressures can be used to vaporize the droplets, forming perfluorocarbon gas bubbles *in situ* that can nucleate inertial cavitation [55]. The bubbles are only formed at the transducer focus, thus localizing the bubble-enhanced heating and ablation to the transducer focal volume.

In this *in vivo* study, accumulation of PSNE in rabbit VX2 tumors was determined as a function of time after injection using T_1-weighted MRI. PSNE was tagged with gadolinium-chelate (Gd), an MR contrast agent, in order to detect it through a change in MR signal intensity. In addition, ultrasound-triggered vaporization of PSNE was tested and an ultrasound imaging system was used to detect the resulting formation of microbubbles. Furthermore, MR thermometry measurements were acquired in order to determine the amount of heating in the tumor with and without PSNE. The overall aim was to investigate the accumulation and activity of PSNE in rabbit VX2 tumors in vivo, in order to assess the potential for PSNE to improve the efficiency and clinical feasibility of MR-guided HIFU for non-invasive treatment of non-resectable solid tumors.

2. METHODS

2.1. Preparation of Phase-Shift Nanoemulsions

Lipids were obtained from Avanti Lipids (Alabaster, AL, USA), gadolinium-diethylenetriaminepentaacetate-bis-oleate (Gd-DTPA-BOA) was purchased from Chemir (Maryland Heights, MO, USA), and the liquid perfluorocarbon was obtained from Fluoromed (Round Rock, TX, USA). Phase-shift nanoemulsions containing gadolinium chelate (Gd-PSNE) were composed of 1,2-dipalmitoyl-sn-glycero-3-phosphocholine (DPPC), 1,2-distearoyl-sn-glycero-3-phosphoethanolamine-N-[amino(polyethylene glycol)-2000] (DSPE-PEG2000), and Gd-DTPA-BOA in a molar ratio of 64:6:30 (DPPC:DSPE-PEG2000:Gd-DTPA-BOA). For HIFU experiments, standard PSNE without Gd-DTPA-BOA were prepared using the same procedure with a molar ratio of 94:6 DPPC:DSPE-PEG2000. Lipids (190 mg) were dissolved in chloroform in a glass round-bottom flask and the solvent was evaporated to form a dry lipid film. After dessicating overnight, the lipid film was rehydrated with 10 ml phosphate-buffered saline (PBS) at 45°C and sonicated for 2 minutes at 20% power using a Vibra-Cell sonicator probe (Sonics & Materials, Newtown, CT, USA) to disperse the lipids. Liquid perfluorocarbon dodecafluoropentane (DDFP, C_5F_{12}) was added to the solution at a volume ratio of 4% and the sample was sonicated in an ice-water bath using the Vibra-Cell sonicator at 25% power in a pulsed sequence of 10 s on, 50 s off, for a total insonation time of 60 s. After sonication, the solution was extruded 16 times through a LIPEX extruder (Northern Lipids, Burnaby, BC, Canada) with polycarbonate membrane filters containing 200 nm pores (Whatman, Piscataway, NJ, USA). The resulting nanoemulsion was dialyzed for 24 hours in 1 L of PBS using 50 kDa dialysis membranes (Spectrum Labs, Rancho Dominguez, CA, USA) in order

to remove any gadolinium chelate that was not incorporated into the perfluorocarbondroplets. The gadolinium concentration in the Gd-PSNE solution was 12 mM before dialysis. PSNE solutions were stored at 4°C until use. Size distribution measurements were acquired at 37°C using dynamic light scattering (90Plus Particle Size Analyzer, Brookhaven Instruments, Holtsville, NY, USA).

2.2. Animals

All animal experiments were performed according to protocols approved by the Harvard Medical School Institutional Animal Care and Use Committee. Two weeks before each experiment, 3×10^7 VX2 cells were injected directly into the left thigh of 3 kg New Zealand white rabbits at a depth of approximately 1 cm. During each experiment, animals were anesthetized with a mixture of ketamine (40 mg/kg body weight, Aveco, Fort Dodge, IA, USA) and xylazine (10 mg/kg body weight, Lloyd Laboratories, Shenandoah, IA, USA). PSNE (0.5 ml/kg body weight) was injected intravenously through a catheter in the ear vein and flushed with 0.5 ml saline. Nine animals were used in this study: four to assess Gd-PSNE accumulation in tumors, one to investigate PSNE vaporization in the tumor, and four to measure HIFU-mediated heating in tumors with and without PSNE.

2.3. Experimental Setup

A diagram of the experimental setup is shown in Figure 2. For all MR imaging experiments, each animal was placed on a custom-built platform in a clinical GE Signa 3T short-bore MRI scanner, oriented so that the tumor was located at the center of a custom-built circular surface MR coil. A custom-built, MR-compatible HIFU transducer (1.5-MHz center frequency, 10-cm aperture, and 8-cm radius of curvature) was placed in a water tank located below the coil. The animal was oriented so that the surface of the tumor-bearing thigh was immersed in the water to ensure adequate acoustic coupling for ultrasound exposures.

T_1-weighted MR images were acquired in all three planes at six time points: before injection of Gd-PSNE and at 0.5, 1, 2, 4, and 6 hours after injection. In each plane, 11-18 images were acquired using a fast spin-echo MR sequence with a pulse repetition time (TR) of 500 ms and echo time (TE) of 13.2 ms. Square 12-cm slices were acquired with a slice thickness of 2 mm and a resolution of 256 × 256 pixels. MR thermometry measurements were acquired using a phase-difference fast spoiled gradient-echo MR sequence with TR of 27 ms and TE of 13.5 ms. Square 8-cm slices were acquired with a slice thickness of 2 mm and a resolution of 256 × 256 pixels. A total of forty temperature maps were acquired at intervals of 3.4 s. To detect changes in the tumor due to thermal damage, T_2-weighted images were acquired using a fast spin-echo sequence with a TR of 4500 ms and a TE of 84.9 ms. Square 12-cm slices were acquired with a slice thickness of 2 mm and a resolution of 256 × 256 pixels.

The HIFU transducer was driven by waveforms produced by a function generator and amplified with an RF power amplifier (240L, E&I, Rochester, NY) that was connected to the HIFU transducer through a BNC connector panel in the wall of the MR control room. Two function generators were used in tandem to generate the ultrasound signals for HIFU ablation experiments. For PSNE vaporization, 100-cycle, 90 W pulses were generated with one arbitrary waveform generator (33220A, Agilent, Santa Clara, CA, USA) at a pulse repetition frequency (PRF) of 670 ms, immediately followed by 1 million-cycle signals at lower acoustic powers (between 5.2 W and 38.5 W) generated by the second arbitrary waveform generator (395, Wavetek, San Diego, CA, USA) to drive inertial cavitation and heat the tumor. The sonication duration was set to either 10 s or 30 s, depending on the acoustic power level. The acoustic output was calibrated using a force balance method [57]. At the beginning of the experiment, the location of the HIFU focus relative to the MRI

coordinates was determined. An agar gel phantom was heated with a 10 W, continuous-wave ultrasound signal for 30 s and an MR thermometry scan was acquired in order to identify the location of peak temperature increase, which was assumed to be the focal point. In a separate experiment without MRI, a 10L5 imaging array on a portable ultrasound system (Terason 2000, Terason, Burlington, MA, USA) was used to acquire B-mode images of PSNE vaporization. All HIFU experiments were performed two hours after PSNE injection.

2.4. MR Data Analysis

To evaluate Gd-PSNE accumulation in rabbit VX2 tumors over time, T_1-weighted MR images were post-processed in MATLAB (Mathworks, Natick, MA, USA). Each image was cropped to isolate the tumor region, Gaussian-filtered, and an intensity threshold was applied. The cutoff value was selected based on the maximum signal intensity in a region of interest within the tumor before PSNE injection. The number of voxels that exceeded the threshold MR signal intensity was counted to determine the total enhanced volume. The dimensions of each voxel were 0.47 mm × 0.47 mm × 2.00 mm.

For MR-guided HIFU experiments, changes in temperature were determined from phase-difference maps as previously described [28]. Thermal dose maps were computed from the temperature maps using Equation 1 [28]:

$$CEM_{43} = \Sigma R^{(43-T)} \Delta t \quad (1)$$

where CEM_{43} represents the cumulative thermal dose in cumulative equivalent minutes at 43°C, R is a constant value of 0.5 for temperatures above 43°C or 0.25 for temperatures below 43°C, and T represents the mean temperature (°C) measured during time Δt (minutes).

3. RESULTS

3.1. Accumulation of Gd-PSNE in Tumor

The size distributions of PSNE in this study were measured with dynamic light scattering and are shown in Figure 3. The mean size of Gd-PSNE was 189 nm and the mean size of standard PSNE (without Gd) was 158 nm. The zeta potential of PSNE was −5.5 ± 14.8 mV. Although standard PSNE could not be detected with MRI, it is expected that the accumulation of standard PSNE in tumors would be comparable to Gd-PSNE because of the similarity in size. In fact, it is possible that greater accumulation of standard PSNE could occur due to the smaller size compared to Gd-PSNE. To study the *in vivo* accumulation of Gd-PSNE in rabbit tumors over time, T_1-weighted MR images were acquired before and after intravenous injection of Gd-PSNE. Representative images of a rabbit tumor with and without Gd-PSNE are shown in Figure 4.

Signal enhancement is evident around the periphery of the tumor, which is expected to have a larger vascular bed and higher perfusion. In the poorly perfused necrotic core, however, significantly less accumulation was observed. This pattern of PSNE accumulation was observed in all MR image slices of tumors with necrotic cores. The total tumor volume with enhanced MR signal after Gd-PSNE injection was determined from T_1-weighted images in four rabbits and is plotted in Figure 5. The total volume with enhanced MR signal increased rapidly in the first 30 minutes after injection of Gd-PSNE, followed by a slight increase over six hours after injection. Because very little change in accumulation was observed between two and six hours after injection, PSNE vaporization and MR-guided HIFU ablation experiments were conducted two hours after PSNE injection.

3.2. HIFU-Mediated Vaporization and Heating in Tumor

To investigate acoustic droplet vaporization (ADV) of PSNE *in vivo*, a 90-W, 67-μs HIFU pulse was transmitted into the rabbit tumor to induce ADV of PSNE, and B-mode ultrasound was used to detect bubble formation. Representative B-mode ultrasound images of the tumor before and after PSNE vaporization are shown in Figure 6. The signal intensity increased at the HIFU focus after the ADV pulse, indicating the presence of bubbles that were formed due to PSNE vaporization. The enhancement is even more noticeable on the corresponding background-subtracted images. The bubbles dissolved into the tissue within a few seconds but that timeframe was sufficient to nucleate acoustic cavitation for bubble-enhanced heating.

To quantify the amount of HIFU-mediated heating in the tumor, MR thermometry measurements were acquired during sonication, and the temperature was calculated at multiple time points. The relative difference in temperature in tumors with PSNE compared to tumors without PSNE is shown in Figure 7 as a function of time during and after sonication using identical ultrasound parameters (acoustic power of 5.2 W). The peak temperature measured in the tumor with PSNE was 60°C, compared to 56°C without PSNE. While the difference in temperature seems minor, the impact on cells and tissue can be significant. For example, Dewhirst et al. [58] demonstrated that increasing the temperature from 55°C to 60°C (+9%) reduced the heating time required for cellular necrosis from 30 sec to 5.1 sec (−83%). In our study, this increase in temperature due to PSNE vaporization was associated with a dramatic increase in the applied thermal dose, which is a better predictor of thermal damage. In the absence of vaporized PSNE, the thermal dose calculated from MR thermometry was 51 equivalent minutes at 43°C. When PSNE was vaporized and the peak temperature was increased to 60°C, the applied thermal dose was increased by a factor of 45 to 2296 equivalent minutes at 43°C. It is evident that for these acoustic parameters, the bubbles dramatically increased the efficiency with which ultrasound was absorbed and the tumor was heated. More importantly, the enhancement in ultrasound-mediated heating led to a reduction in the acoustic power required for lesion formation within the tumors. To illustrate this, thermal dose maps are shown in Figure 8 with three different sonication parameters. Previous studies have noted that lesions form when the thermal dose exceeds a critical threshold value [59, 60]. Using a critical thermal dose threshold of 240 CEM_{43} that correlated with lesion formation in previous studies [61, 62], contour lines were drawn to indicate the expected lesion outline. This metric indicates that lesions can be formed at lower acoustic powers with PSNE. As shown in Figure 8A, with a 10-second sonication at 15.7 W, an area of 2.1 mm^2 exceeded 240 CEM_{43} in a tumor with PSNE. In a tumor without PSNE, however, there was no area that reached 240 CEM_{43} with a 10-second sonication at 16.5 W. Without vaporized PSNE, the applied acoustic power had to be increased by 245% to 38.5 W in order to heat a comparable area (3.1 mm^2) beyond a thermal dose of 240 CEM_{43}. These results clearly show the effect of bubbles formed in tumors via PSNE vaporization on MRgFUS-mediated tumor ablation.

4. DISCUSSION

The results of this study demonstrate that Gd-PSNE can accumulate in rabbit tumors for at least six hours after intravenous injection. This suggests that the time window for conducting HIFU ablations after a single PSNE injection is large (on the order of hours). In contrast, microbubble-enhanced HIFU ablation requires continuous infusion or repeated injections due to lack of microbubble accumulation in tumors and rapid clearance from circulation (half-life < 5 min). MR signal enhancement (indicating the presence of Gd-PSNE) was most evident around the tumor rim and appeared to gradually diffuse further into the tumor over time, but enhancement was not observed at the center of the tumor. This is

likely due to the fact that the center of the tumor is typically poorly perfused and necrotic in advanced VX2 tumors, which could pose a challenge to the delivery of therapeutic agents and nanoparticles [63-65]. In contrast, the tumor rim is generally highly vascularized and contains the majority of the viable cancer cells, which would be more easily targeted through the EPR effect [66]. More importantly, PSNE collected within highly vascularized regions could be vaporized to form microbubbles that dramatically enhanced HIFU-mediated heating, thus counteracting the cooling effects provided by circulating blood. Furthermore, HIFU-mediated ablation is problematic throughout well-perfused tissues, such as the periphery of tumors, due to cooling effects of circulating blood. Similar to other nanoparticles, PSNE accumulates predominately in the tumor periphery, seeding highly vascularized regions with nuclei for inertial cavitation, which can be used to enhance HIFU-mediated ablation as well as destroy vessels that feed tumors. Ultimately, this will reduce blood perfusion in solid tumors, potentially leading to an improvement in the efficiency of HIFU-induced heating in the tumor core. It is important to note that HIFU ablation treatments require constant monitoring and adjustment of the transmitted acoustic power and sonication duration in order to adequately ablate the targeted structures. This will also be necessary with PSNE, but inertial cavitation emissions from vaporized PSNE can potentially be monitored to serve as an additional feedback parameter [67-69].

HIFU-mediated vaporization of PSNE was observed with B-mode ultrasound imaging of the tumor two hours after intravenous injection of PSNE. Previous studies have used microbubbles administered systemically in order to enhance HIFU-mediated heating. However, this approach is limited by the rapid clearance time (on the order of minutes) and the fact that the size of the microbubbles (microns) prevents extravasation through tumor vessels. As an alternative to microbubbles, Zhang *et al.* [70] studied lesion formation in canine liver using perfluorocarbon droplets with diameters greater than a micron. Most likely, those droplets were vaporized within the tumor vasculature, whereas the nanoemulsion droplets used in this study were small enough (diameter < 200 nm) to extravasate through leaky tumor vessel walls and accumulate within the tumor interstitium and reside for hours. This study was the first *in vivo* demonstration that PSNE could be vaporized *within* solid tumors and the resultant bubbles driven acoustically to enhance HIFU-mediated heating.

The long-term goal is to use PSNE to decrease the acoustic pressure and treatment time required to ablate solid tumors, in order to improve the clinical feasibility and safety of MR-guided HIFU for non-invasive treatment of non-resectable solid tumors. Previous studies have reported adverse events that were observed with HIFU ablation treatments, in particular skin burns [31, 32]. It is anticipated that skin burns (and potentially other adverse events) will be reduced by using PSNE to lower the acoustic pressures required to ablate tumors, thereby increasing the safety of this procedure. Future studies will seek to improve detection and activation of PSNE for ultrasound-mediated ablation of solid tumors, but the results of the current pilot *in vivo* study suggest that PSNE may enhance the efficiency of MR-guided HIFU for treatment of non-resectable solid tumors.

5. CONCLUSIONS

It was found with T_1-weighted MRI that gadolinium-tagged PSNE accumulated in rabbit VX2 tumors for at least six hours after intravenous injection. B-mode ultrasound imaging revealed that PSNE were vaporized into microbubbles *in vivo* using short HIFU pulses. Furthermore, MR thermometry measurements showed that PSNE enhanced HIFU-mediated heating in rabbit tumors. These results suggest that PSNE may potentially improve the clinical feasibility of MR-guided HIFU by reducing the treatment times and acoustic intensities required.

Acknowledgments

This work was supported by a grant from the National Institutes of Health (R21 EB009493).

REFERENCES

[1]. Murphy, SL.; Xu, J.; Kochanek, KD. National Vital Statistics Report. 2012. Deaths: Preliminary data for 2010; p. 60

[2]. SEER cancer statistics review 1975-2008. National Cancer Institute;

[3]. Dodd GD 3rd, Soulen MC, Kane RA, Livraghi T, Lees WR, Yamashita Y, Gillams AR, Karahan OI, Rhim H. Minimally invasive treatment of malignant hepatic tumors: At the threshold of a major breakthrough. Radiographics. 2000; 201:9–27. [PubMed: 10682768]

[4]. Liu C, Frilling A, Dereskewitz C, Broelsch CE. Tumor seeding after fine needle aspiration biopsy and percutaneous radiofrequency thermal ablation of hepatocellular carcinoma. Digestive Radiology. 2003; 20:460–463.

[5]. Nagaoka Y, Nakayama R, Iwata M. Cutaneous seeding following percutaneous ethanol injection therapy for hepatocellular carcinoma. Intern Med. 2004; 433:268–269. [PubMed: 15098615]

[6]. Fry FJ, Heimburger RF, Gibbons LV, Eggleton RC. Ultrasound for visualization and modification of brain tissue. IEEE Transactions on Sonics and Ultrasonics. 1970; 173:165–169.

[7]. Fry W, Fry WJ, Wulff VJ. Physical factors involved in ultrasonically induced changes in living systems: II. amplitude duration relations and the effect of hydrostatic pressure for nerve tissue. J. Acoust. Soc. Am. 1951; 23:364–368.

[8]. Kennedy JE. High-intensity focused ultrasound in the treatment of solid tumours. Nat Rev Cancer. 2005; 54:321–327. [PubMed: 15776004]

[9]. ter Haar G, Coussios C. High intensity focused ultrasound: Past, present and future. Int J Hyperthermia. 2007; 232:85–87.

[10]. Wall PD, Tucker D, Fry FJ, Mosberg WH Jr. The use of high intensity ultrasound in experimental neurology. J. Acoust. Soc. Am. 1953; 25:281–285.

[11]. Wu F, Wang ZB, Chen WZ, Wang W, Gui Y, Zhang M, Zheng G, Zhou Y, Xu G, Li M, Zhang C, Ye H, Feng R. Extracorporeal high intensity focused ultrasound ablation in the treatment of 1038 patients with solid carcinomas in china: An overview. Ultrason Sonochem. 2004; 113-4:149–154. [PubMed: 15081972]

[12]. tar Haar G, Coussios C. High intensity focused ultrasound: Physical principles and devices. Int J Hyperthermia. 2007; 232:89–104.

[13]. Wu F, Wang ZB, Cao YD, Chen WZ, Bai J, Zou JZ, Zhu H. A randomised clinical trial of high-intensity focused ultrasound ablation for the treatment of patients with localised breast cancer. Br J Cancer. 2003; 8912:2227–2233. [PubMed: 14676799]

[14]. Wu F, Wang ZB, Zhu H, Chen WZ, Zou JZ, Bai J, Li KQ, Jin CB, Xie FL, Su HB. Extracorporeal high intensity focused ultrasound treatment for patients with breast cancer. Breast Cancer Res Treat. 2005; 921:51–60. [PubMed: 15980991]

[15]. Wu F, Wang ZB, Zhu H, Chen WZ, Zou JZ, Bai J, Li KQ, Jin CB, Xie FL, Su HB. Feasibility of US-guided high-intensity focused ultrasound treatment in patients with advanced pancreatic cancer: Initial experience. Radiology. 2005; 2363:1034–1040. [PubMed: 16055692]

[16]. Illing RO, Kennedy JE, Wu F, ter Haar GR, Protheroe AS, Friend PJ, Gleeson FV, Cranston DW, Phillips RR, Middleton MR. The safety and feasibility of extracorporeal high-intensity focused ultrasound (HIFU) for the treatment of liver and kidney tumours in a western population. Br J Cancer. 2005; 938:890–895. [PubMed: 16189519]

[17]. Kennedy JE, Wu F, ter Haar GR, Gleeson FV, Phillips RR, Middleton MR, Cranston D. High-intensity focused ultrasound for the treatment of liver tumours. Ultrasonics. 2004; 421-9:931–935. [PubMed: 15047409]

[18]. Wu F, Wang ZB, Chen WZ, Bai J, Zhu H, Qiao TY. Preliminary experience using high intensity focused ultrasound for the treatment of patients with advanced stage renal malignancy. J Urol. 2003; 1706(Pt 1):2237–2240. [PubMed: 14634387]

[19]. Poissonnier L, Chapelon JY, Rouviere O, Curiel L, Bouvier R, Martin X, Dubernard JM, Gelet A. Control of prostate cancer by transrectal HIFU in 227 patients. Eur Urol. 2007; 512:381–387. [PubMed: 16857310]

[20]. Sanghvi NT, Foster RS, Bihrle R, Casey R, Uchida T, Phillips MH, Syrus J, Zaitsev AV, Marich KW, Fry FJ. Noninvasive surgery of prostate tissue by high intensity focused ultrasound: An updated report. Eur J Ultrasound. 1999; 91:19–29. [PubMed: 10099163]

[21]. Uchida T, Sanghvi NT, Gardner TA, Koch MO, Ishii D, Minei S, Satoh T, Hyodo T, Irie A, Baba S. Transrectal high-intensity focused ultrasound for treatment of patients with stage T1b-2n0m0 localized prostate cancer: A preliminary report. Urology. 2002; 593:394–8. discussion 398-9. [PubMed: 11880077]

[22]. Kopelman D, Papa M. Magnetic resonance-guided focused ultrasound surgery for the noninvasive curative ablation of tumors and palliative treatments: A review. Ann Surg Oncol. 2007; 145:1540–1550. [PubMed: 17318277]

[23]. Chen JC, Moriarty JA, Derbyshire JA, Peters RD, Trachtenberg J, Bell SD, Doyle J, Arrelano R, Wright GA, Henkelman RM, Hinks RS, Lok SY, Toi A, Kucharczyk W. Prostate cancer: MR imaging and thermometry during microwave thermal ablation-initial experience. Radiology. 2000; 2141:290–297. [PubMed: 10644139]

[24]. Hazle JD, Diederich CJ, Kangasniemi M, Price RE, Olsson LE, Stafford RJ. MRI-guided thermal therapy of transplanted tumors in the canine prostate using a directional transurethral ultrasound applicator. J Magn Reson Imaging. 2002; 154:409–417. [PubMed: 11948830]

[25]. Hazle JD, Stafford RJ, Price RE. Magnetic resonance imaging-guided focused ultrasound thermal therapy in experimental animal models: Correlation of ablation volumes with pathology in rabbit muscle and VX2 tumors. J Magn Reson Imaging. 2002; 152:185–194. [PubMed: 11836775]

[26]. Kangasniemi M, Diederich CJ, Price RE, Stafford RJ, Schomer DF, Olsson LE, Tyreus PD, Nau WH, Hazle JD. Multiplanar MR temperature-sensitive imaging of cerebral thermal treatment using interstitial ultrasound applicators in a canine model. J Magn Reson Imaging. 2002; 165:522–531. [PubMed: 12412028]

[27]. McDannold N, Vykhodtseva N, Jolesz FA, Hynynen K. MRI investigation of the threshold for thermally induced blood-brain barrier disruption and brain tissue damage in the rabbit brain. Magn Reson Med. 2004; 515:913–923. [PubMed: 15122673]

[28]. McDannold NJ, King RL, Jolesz FA, Hynynen KH. Usefulness of MR imaging-derived thermometry and dosimetry in determining the threshold for tissue damage induced by thermal surgery in rabbits. Radiology. 2000; 2162:517–523. [PubMed: 10924580]

[29]. Peters RD, Chan E, Trachtenberg J, Jothy S, Kapusta L, Kucharczyk W, Henkelman RM. Magnetic resonance thermometry for predicting thermal damage: An application of interstitial laser coagulation in an in vivo canine prostate model. Magn Reson Med. 2000; 446:873–883. [PubMed: 11108624]

[30]. Sherar MD, Moriarty JA, Kolios MC, Chen JC, Peters RD, Ang LC, Hinks RS, Henkelman RM, Bronskill MJ, Kucharcyk W. Comparison of thermal damage calculated using magnetic resonance thermometry, with magnetic resonance imaging post-treatment and histology, after interstitial microwave thermal therapy of rabbit brain. Phys Med Biol. 2000; 4512:3563–3576. [PubMed: 11131184]

[31]. Yu T, Luo J. Adverse events of extracorporeal ultrasound-guided high intensity focused ultrasound therapy. PLoS One. 2011; 612:e26110. [PubMed: 22194777]

[32]. Yu T, Huang P. Extracorporeal ultrasound-guided high intensity focused ultrasound therapy: Present limitations. African Journal of Pharmacy and Pharmacology. 2011; 512:1501–1507.

[33]. Clarke RL, ter Haar GR. Temperature rise recorded during lesion formation by high-intensity focused ultrasound. Ultrasound Med Biol. 1997; 232:299–306. [PubMed: 9140186]

[34]. Holt RG, Roy RA. Measurements of bubble-enhanced heating from focused, MHz-frequency ultrasound in a tissue-mimicking material. Ultrasound Med Biol. 2001; 2710:1399–1412. [PubMed: 11731053]

[35]. Hynynen K. The threshold for thermally significant cavitation in dog's thigh muscle in vivo. Ultrasound Med Biol. 1991; 172:157–169. [PubMed: 2053212]

[36]. Umemura S, Kawabata K, Sasaki K. In vivo acceleration of ultrasonic tissue heating by microbubble agent. IEEE Trans Ultrason Ferroelectr Freq Control. 2005; 5210:1690–1698. [PubMed: 16382620]

[37]. Luo W, Zhou X, He G, Li Q, Zheng X, Fan Z, Liu Q, Yu M, Han Z, Zhang J, Qian Y. Ablation of high intensity focused ultrasound combined with SonoVue on rabbit VX2 liver tumors: Assessment with conventional gray-scale US, conventional color/power doppler US, contrast-enhanced color doppler US, and contrast-enhanced pulse-inversion harmonic. US Ann Surg Oncol. 2008; 1510:2943–2953.

[38]. Luo W, Zhou X, Ren X, Zheng M, Zhang J, He G. Enhancing effects of SonoVue, a microbubble sonographic contrast agent, on high-intensity focused ultrasound ablation in rabbit livers in vivo. J Ultrasound Med. 2007; 264:469–476. [PubMed: 17384044]

[39]. Luo W, Zhou X, Yu M, He G, Zheng X, Li Q, Liu Q, Han Z, Zhang J, Qian Y. Ablation of high-intensity focused ultrasound assisted with SonoVue on rabbit VX2 liver tumors: Sequential findings with histopathology, immunohistochemistry, and enzyme histochemistry. Ann Surg Oncol. 2009; 168:2359–2368. [PubMed: 19475452]

[40]. McDannold NJ, Vykhodtseva NI, Hynynen K. Microbubble contrast agent with focused ultrasound to create brain lesions at low power levels: MR imaging and histologic study in rabbits. Radiology. 2006; 2411:95–106. [PubMed: 16990673]

[41]. Chung DJ, Cho SH, Lee JM, Hahn ST. Effect of microbubble contrast agent during high intensity focused ultrasound ablation on rabbit liver in vivo. Eur J Radiol. 2012; 814:e519–23. [PubMed: 21708438]

[42]. Yu T, Hu D, Xu C. Microbubbles improve the ablation efficiency of extracorporeal high intensity focused ultrasound against kidney tissues. World J Urol. 2008; 266:631–636. [PubMed: 18594828]

[43]. Charrois GJ, Allen TM. Rate of biodistribution of STEALTH liposomes to tumor and skin: Influence of liposome diameter and implications for toxicity and therapeutic activity. Biochim Biophys Acta. 2003; 16091:102–108. [PubMed: 12507764]

[44]. Ishida O, Maruyama K, Sasaki K, Iwatsuru M. Size-dependent extravasation and interstitial localization of polyethyleneglycol liposomes in solid tumor-bearing mice. Int J Pharm. 1999; 1901:49–56. [PubMed: 10528096]

[45]. Yuan F, Dellian M, Fukumura D, Leunig M, Berk DA, Torchilin VP, Jain RK. Vascular permeability in a human tumor xenograft: Molecular size dependence and cutoff size. Cancer Res. 1995; 5517:3752–3756. [PubMed: 7641188]

[46]. Sokka SD, King R, Hynynen K. MRI-guided gas bubble enhanced ultrasound heating in in vivo rabbit thigh. Phys Med Biol. 2003; 482:223–241. [PubMed: 12587906]

[47]. Melodelima D, Chapelon JY, Theillere Y, Cathignol D. Combination of thermal and cavitation effects to generate deep lesions with an endocavitary applicator using a plane transducer: Ex vivo studies. Ultrasound Med Biol. 2004; 301:103–111. [PubMed: 14962614]

[48]. Church CC. Spontaneous homogeneous nucleation, inertial cavitation and the safety of diagnostic ultrasound. Ultrasound Med Biol. 2002; 2810:1349–1364. [PubMed: 12467862]

[49]. Xu Z, Fowlkes JB, Ludomirsky A, Cain CA. Investigation of intensity thresholds for ultrasound tissue erosion. Ultrasound Med Biol. 2005; 3112:1673–1682. [PubMed: 16344129]

[50]. Kripfgans OD, Fabiilli ML, Carson PL, Fowlkes JB. On the acoustic vaporization of micrometer-sized droplets. J Acoust Soc Am. 2004; 1161:272–281. [PubMed: 15295987]

[51]. Kripfgans OD, Fowlkes JB, Miller DL, Eldevik OP, Carson PL. Acoustic droplet vaporization for therapeutic and diagnostic applications. Ultrasound Med Biol. 2000; 267:1177–1189. [PubMed: 11053753]

[52]. Kripfgans OD, Fowlkes JB, Woydt M, Eldevik OP, Carson PL. In vivo droplet vaporization for occlusion therapy and phase aberration correction. IEEE Trans Ultrason Ferroelectr Freq Control. 2002; 496:726–738. [PubMed: 12075966]

[53]. Schadlich A, Caysa H, Mueller T, Tenambergen F, Rose C, Gopferich A, Kuntsche J, Mader K. Tumor accumulation of NIR fluorescent PEG-PLA nanoparticles: Impact of particle size and human xenograft tumor model. ACS Nano. 2011; 511:8710–8720. [PubMed: 21970766]

[54]. Maeda H, Wu J, Sawa T, Matsumura Y, Hori K. Tumor vascular permeability and the EPR effect in macromolecular therapeutics: A review. J Control Release. 2000; 651-2:271–284. [PubMed: 10699287]

[55]. Zhang P, Porter T. An in vitro study of a phase-shift nanoemulsion: A potential nucleation agent for bubble-enhanced HIFU tumor ablation. Ultrasound Med Biol. 2010; 3611:1856–1866. [PubMed: 20888685]

[56]. Kopechek JA, Zhang P, Burgess MT, Porter TM. Synthesis of phase-shift nanoemulsions with narrow size distributions for acoustic droplet vaporization and bubble-enhanced heating. J. Vis. Exp. 2012; 67:e4308. [PubMed: 23007836]

[57]. Maruvada S, Harris GR, Herman BA, King RL. Acoustic power calibration of high-intensity focused ultrasound transducers using a radiation force technique. J Acoust Soc Am. 2007; 1213:1434–1439. [PubMed: 17407880]

[58]. Dewhirst MW, Viglianti BL, Lora-Michiels M, Hanson M, Hoopes PJ. Basic principles of thermal dosimetry and thermal thresholds for tissue damage from hyperthermia. Int J Hyperthermia. 2003; 193:267–294. [PubMed: 12745972]

[59]. Haemmerich D, Webster JG, Mahvi DM. Thermal dose versus isotherm as lesion boundary estimator for cardiac and hepatic radio-frequency ablation. IEEE EMBS Proceedings. 2003; 1:134–137.

[60]. Graham SJ, Chen L, Leitch M, Peters RD, Bronskill MJ, Foster FS, Henkelman RM, Plewes DB. Quantifying tissue damage due to focused ultrasound heating observed by MRI. Magn Reson Med. 1999; 412:321–328. [PubMed: 10080280]

[61]. McDannold, Hynynen K, Wolf D, Wolf G, Jolesz F. MRI evaluation of thermal ablation of tumors with focused ultrasound. J Magn Reson Imaging. 1998; 81:91–100. [PubMed: 9500266]

[62]. Chung AH, Jolesz FA, Hynynen K. Thermal dosimetry of a focused ultrasound beam in vivo by magnetic resonance imaging. Med Phys. 1999; 269:2017–2026. [PubMed: 10505893]

[63]. Weinberg BD, Ai H, Blanco E, Anderson JM, Gao J. Antitumor efficacy and local distribution of doxorubicin via intratumoral delivery from polymer millirods. J Biomed Mater Res A. 2007; 811:161–170. [PubMed: 17120197]

[64]. Lewandowski RJ, Eifler AC, Bentrem DJ, Chung JC, Wang D, Woloschak GE, Yang GY, Ryu R, Salem R, Larson AC, Omary RA. Functional magnetic resonance imaging in an animal model of pancreatic cancer. World J Gastroenterol. 2010; 1626:3292–3298. [PubMed: 20614485]

[65]. Chen X, Barkauskas KJ, Weinberg BD, Duerk JL, Abdul-Karim FW, Paul S, Saidel GM. Dynamics of MRI-guided thermal ablation of VX2 tumor in paraspinal muscle of rabbits. IEEE Trans Biomed Eng. 2008; 553:1004–1014. [PubMed: 18334392]

[66]. Brannon-Peppas L, Blanchette JO. Nanoparticle and targeted systems for cancer therapy. Adv Drug Deliv Rev. 2004; 5611:1649–1659. [PubMed: 15350294]

[67]. Jensen CR, Ritchie RW, Gyongy M, Collin JR, Leslie T, Coussios CC. Spatiotemporal monitoring of high-intensity focused ultrasound therapy with passive acoustic mapping. Radiology. 2012; 2621:252–261. [PubMed: 22025731]

[68]. Haworth KJ, Mast TD, Radhakrishnan K, Burgess MT, Kopechek JA, Huang SL, McPherson DD, Holland CK. Passive imaging with pulsed ultrasound insonations. J Acoust Soc Am. 2012; 1321:544–553. [PubMed: 22779500]

[69]. Salgaonkar VA, Datta S, Holland CK, Mast TD. Passive cavitation imaging with ultrasound arrays. J Acoust Soc Am. 2009; 1266:3071–3083. [PubMed: 20000921]

[70]. Zhang M, Fabiilli ML, Haworth KJ, Padilla F, Swanson SD, Kripfgans OD, Carson PL, Fowlkes JB. Acoustic droplet vaporization for enhancement of thermal ablation by high intensity focused ultrasound. Acad Radiol. 2011; 189:1123–1132. [PubMed: 21703883]

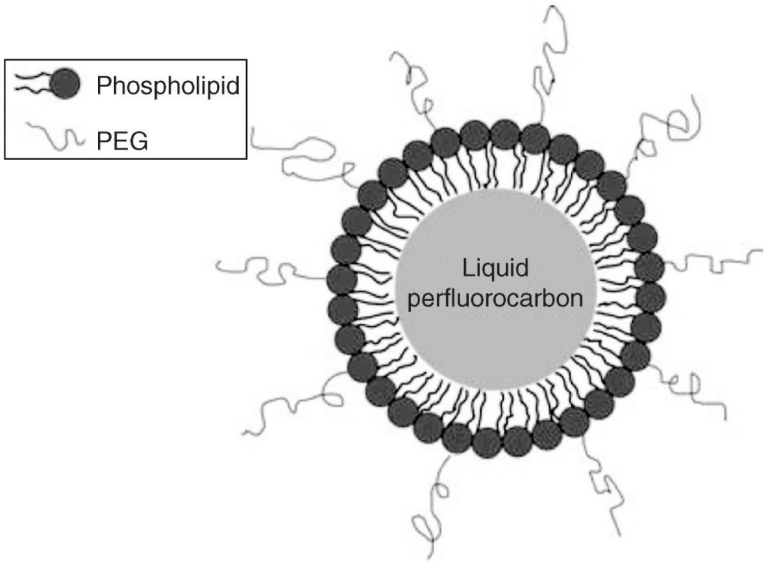

Figure 1.
Illustration of a perfluorocarbon droplet in PSNE. A droplet is composed of a liquid perfluorocarbon core surrounded by a phospholipid shell containing polyethylene glycol (PEG) to improve stability in vivo.

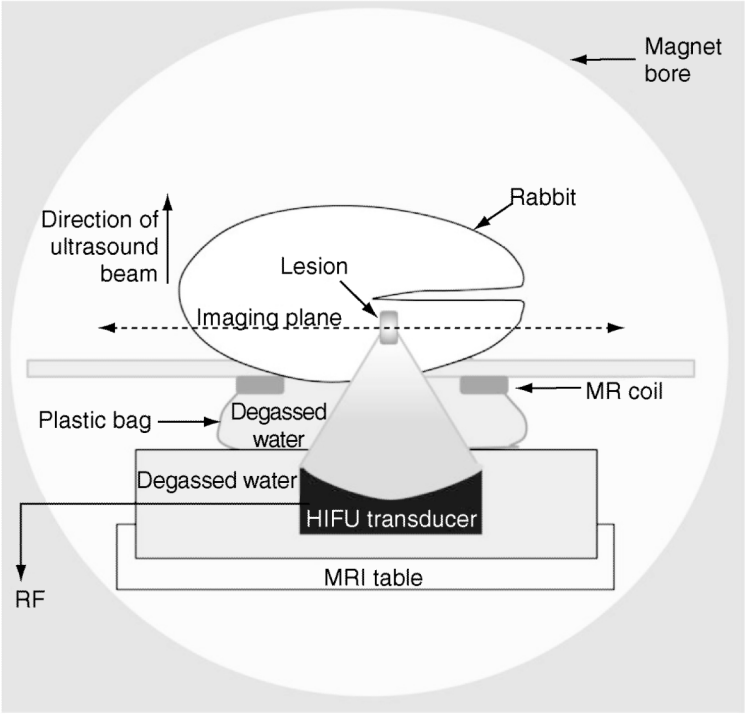

Figure 2.
Setup for HIFU experiments.

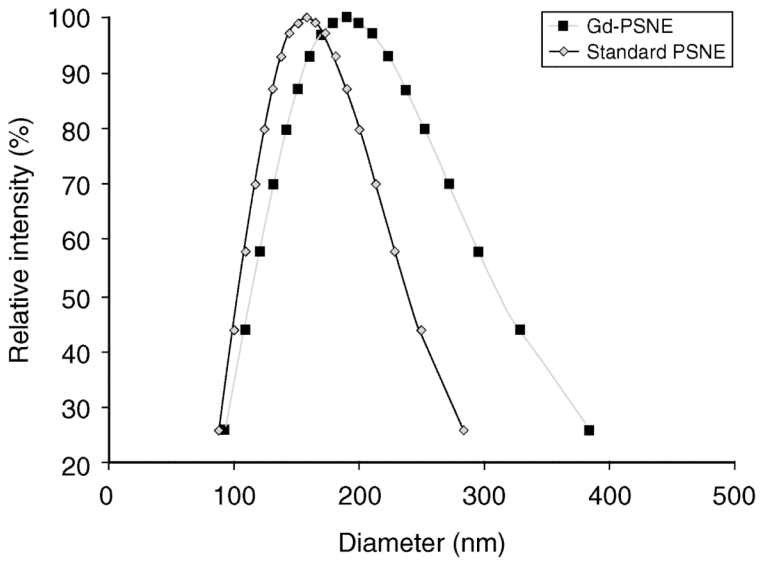

Figure 3.

Size distribution of Gd-PSNE and standard PSNE, measured with dynamic light scattering. The units of the ordinate axes are based on the intensity of scattered light from particles of a certain size relative to the total scattered light intensity from the sample.

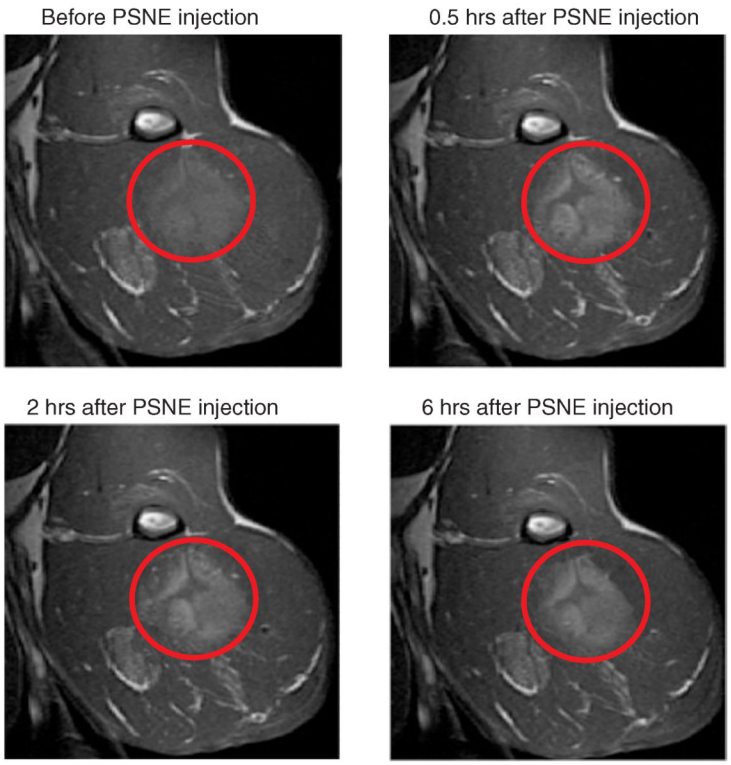

Figure 4.
Representative T_1-weighted MR images of Gd-PSNE accumulation in tumor as a function of time after injection. Signal enhancement from Gd-PSNE accumulation is evident throughout the periphery of the tumor (indicated with red circles).

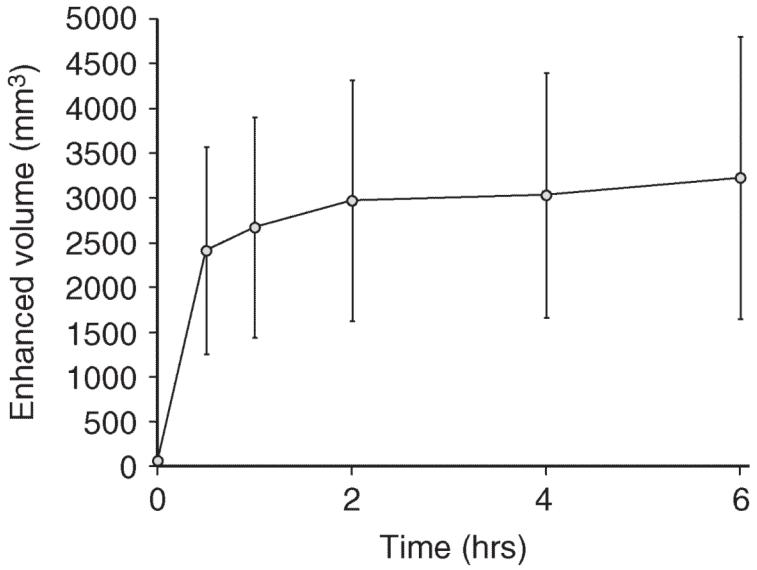

Figure 5.
Total tumor volume with enhanced MR signal from Gd-PSNE as a function of time after injection. Error bars represent the standard deviation from four rabbits.

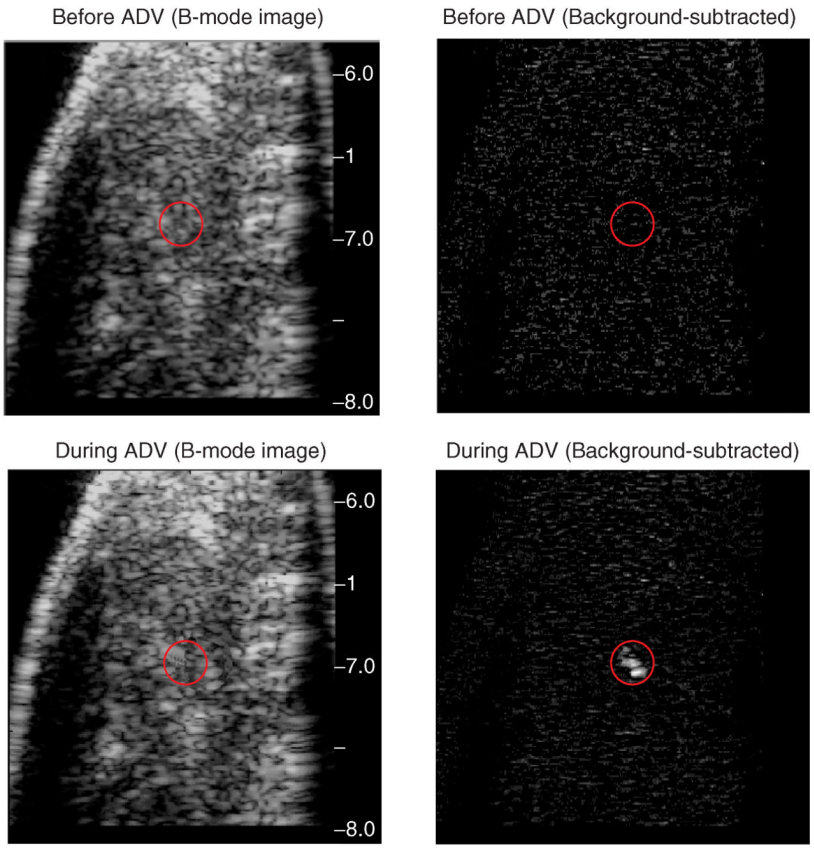

Figure 6.
Representative B-mode and background-subtracted images of PSNE vaporization *in vivo*. The red circles indicate the location of the HIFU focus. The appearance of microbubbles due to PSNE vaporization is evident by the enhanced brightness at the focus during acoustic droplet vaporization (ADV).

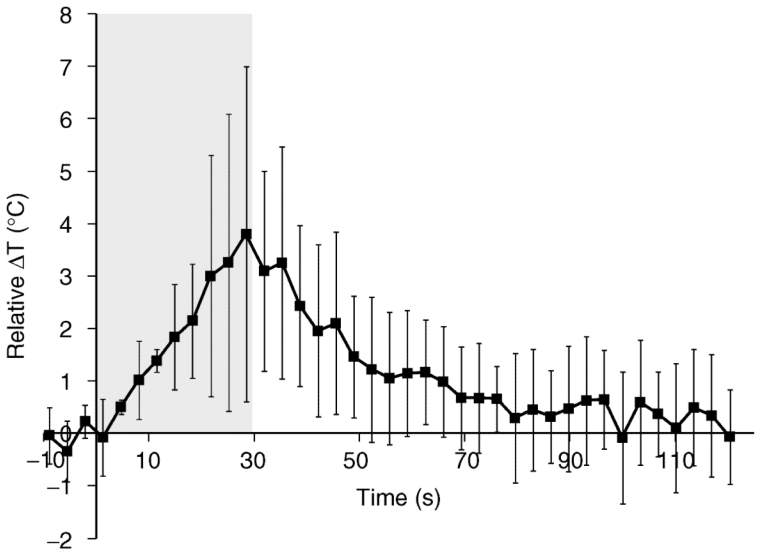

Figure 7.

Relative difference in temperature due to HIFU-mediated heating with and without PSNE, plotted as a function of time during and after sonication. The gray box indicates the time when the tumor was sonicated with an acoustic power of 5.2 W. Error bars represent the standard deviation of the data from three rabbits.

Figure 8.

Thermal dose maps from HIFU treatments in tumors with and without PSNE, plotted in units of cumulative equivalent minutes (CEM) at 43°C. Red contours outline the area where the thermal dose exceeded 240 CEM_{43}. (A) Tumor with PSNE, sonicated for 10 seconds at an acoustic power of 15.7 W. (B) Tumor without PSNE, sonicated for 10 seconds at an acoustic power of 16.5 W. (C) Tumor without PSNE, sonicated for 10 seconds at an acoustic power of 38.5 W.